OLDC-NET: OPTIMIZED RECURRENT CONVOLUTIONAL NEURAL NETWORK-BASED LUNG DISEASE DETECTION AND CLASSIFICATION

[1]N. SUDHIR REDDY and [2]Dr. V. KHANAA

[1]Research Scholar, [2]Professor, Dean Information,
[1,2] Department of Computer Science and Engineering, Bharath Institute of Higher Education and Research (BIHER), Chennai, Tamil Nadu.
[1] E-mail: sudhir.navar@mrce.in

Abstract:

Lung cancer is a critical illness that kills millions of people worldwide. As a result, early diagnosis and categorization of lung tumors has the potential to save millions of lives. However, traditional approaches failed to provide superior categorization results. Thus, this article is focused artificial intelligence approach with optimized lung disease classification network (OLDC-Net) for multi class classification. Initially, hybrid recursive box filtering (HRBF) is used to perform the preprocessing of the Computed Tomography (CT) based lung images. Then, segmentation of lung cancer is performed using Unified-K-Means clustering (UKMC) operation, which locates the cancer effected region. Further, features are extracted using multi-level discrete wavelet transform (ML-DWT), which contains the disease specific information. Finally, natural inspired moth-swarm optimization algorithm (MSOA) is used for feature selection operation, which select the best features from available features. Finally, recurrent convolutional neural network (RCNN) is used to perform the classification of lung cancers with benign, malignant lung types. The simulation results shows that the proposed OLDC-Net resulted in superior segmentation, classification performance as compared to conventional methods.

Keywords: Computed tomography lung images, lung disease detection and classification, hybrid recursive box filtering, K-Means clustering, K-Means clustering, recurrent convolutional neural network.

1. INTRODUCTION

Lung cancer is a critical form of cancer that affects millions of individuals throughout the globe. The recent COVID-19 epidemic has also resulted in an extraordinary increase in lung ailments. Furthermore, there is a direct association between COVID-19 and lung cancer [1], since people with lung cancer are more likely to be affected by COVID-19. Lung cancer segmentation and categorization is an important topic of research, and several studies have been conducted [2]. As a result, early diagnosis and categorization of lung malignancies may save the lives of millions of individuals. However, hospitals are still employing older approaches such as clinical trials to diagnose advanced stage lung cancer [3]. However, conventional techniques use more time with nominal accuracy. As a result, there is a significant need to adopt computer-aided design (CAD) systems in hospitals and labs.

Traditional CAD systems [4] use simple image processing algorithms with little intelligence, resulting in inferior segmentation and classification results. CAD systems are now being created using artificial intelligence technologies such as machine learning and deep learning algorithms.

However, traditional machine learning models suffer from excessive computational complexity and poor classification performance. As a result, deep learning models must be used in CAD systems rather than machine learning methodologies. In order to create a dataset for segmentation, we used the RCNN [5] for lung image classification and the morphological graph cut approach for label creation on the obtained images. There was no need to do any manual labelling operations in order to create the dataset for pretraining. Computer vision and medical imaging technologies are utilized in combination to build CADs [6] for lung segmentation and classification. Lung parenchyma segmentation is utilized as a pre-processing phase in lung CT image processing, which is highly important in the area of lung disease.

Pre-processing [7] procedures have a direct impact on the final CT scan preparation. As a result, faster and more accurate segmentation processes for lung CT images are an intriguing subject worth investigating, with urgent actual requirement and therapeutic relevance. Several lung division processes have been studied, and a portion of the standard ways use threshold region-development techniques [8]. Regardless, the outcomes are unimpressive, and the method is time-consuming and labor-intensive. As a result, it is still regarded an unknown territory.

The division is finished fast, but the quality is poor since the predicted dimensions of the lung boundaries are the same as those of the windpipe and bronchus region. Deep learning [9] is a basic image-segmentation method that is dependent on the region of the CT scan. It has the capacity to separate the interstitial lung boundaries swiftly and effectively. While this method is successful, it takes time and the evolving model is sensitive to boundary circumstances. The majority of lung segmentation frameworks in use today are hybrid systems that combine an edge-respecting method with unexpected development and other extraction techniques. In the presence of a lung infection, a number of tests are done based on the division of the lung parenchyma. As a result, the following are the main contributions of this article:

- Initially, HRBF is used to reduce various sorts of noise from lung CT scans while simultaneously enhancing the cancer area.
- The region of interest of cancer is then localized using UKMC based segmentation.
- Further, MLDWT-is used for feature extraction and MSOA based meta hysteresis is used for best feature selection.
- Finally, RCNN is a model that performs training and testing operations on extracted features and classifies benign and malignant lung tumors.

The following people contributed to the rest of the article: Section 2 is concerned with the associated work with their issue description. Section 3 is devoted to a thorough examination of the planned OLDC-Net. Section 4 deals with results and discussion and comparison with conventional approaches. Section 5 concludes the article with the possible future enhancements.

2. LITERATURE SURVEY

There are several medical imaging modalities, each with its own set of distinct properties. This also aids in the evolution of processing techniques. The multi-scale CT scan categorization technique is frequently used in the scientific community. Several research surveys focused [10] on CT scan-based lung cancer diagnosis and categorization are being done. According to the report, machine learning models diminish classification accuracy and result in incorrect categorization.

The authors of [11] presented a variety of evolutionary approaches for lung segmentation using a mean filtering-based preprocessing procedure. Four high-quality algorithms were used to pre-processed CT images to increase their overall quality. MATLAB was used to evaluate the results to verify realistic findings for 20 sample lung scans. This approach's computational complexity [12] still needs to be decreased. Furthermore, the authors of [13] focused on lung cancer diagnostics using enhanced techniques. In this study, median filter-based denoising with threshold segmentation improved the accuracy of the preprocessing by Gaussian filter [14] of these photographs, leading to the invention of an algorithm. This technique is far more sensitive, specific, precise, and accurate than prior approaches, with a lower number of false positives.

The authors of [15] concentrated on the implementation of bilateral filter-based preprocessing with random forest classification. Image categorization is the process of combining pertinent data from several input CT scans into a single, clearly segmented image that is then shown. As a consequence, trilateral filter [16] based preprocessing is used in CT scan preprocessing to generate noise-free images. Based on available characteristics, lung cancer classification strategies may be divided into two categories: spatial-domain image classification methods and transform-domain image preprocessing methods such as non-local means (NLM) [17].

Multi-scale image segmentation and classification approaches [18] such as pyramid-based classification, as well as a variety of other multi-scale image classification algorithms, are currently in use. Changing parameters provide essential information for each of the tactics mentioned in [19]. When the derived details are segmented together as a consequence of measuring the parameters, detailed relevant information is acquired together with the segmented CT scan. The authors of [20] employed fundamental morphological methodologies for CT image segmentation, which resulted in good performance for benign illnesses but not for malignant disorders. Image segmentation applications such as adaptive thresholding [21], comprising super-resolution processing, denoising, and segmentation, are becoming more common.

With good cause, the SR theory has sparked a lot of attention in the field of image processing in recent years, notably in the context of image categorization [22]. For lung image segmentation, we all know that Fuzzy c-means clustering (FCM) [23] and Modified OTSU (MOTSU) [24] may be used to create dictionaries for traditional SR techniques. Traditional SR methods that employ a set vocabulary, on the other hand, have a lot of restrictions when it comes to CT scan categorization. [25] Suggested an SVM model for image classification and

denoising that can produce an adaptive compressed lexicon for CT scan categorization by merging images from multiple sources. According to the researchers [26], this technique may bring the modified spatial frequency with k-means clustering (UKMC) utilized for lung image segmentation, as well as the core idea of an adaptive selection dictionary, to SR.

Based on artificial intelligence models, two redundant wavelet transformations were used for lung cancer classification with multi-view medical imaging: Redundant Wavelet Transform (RWT) based support vector machine (SVM) [27] and Redundant Discrete Wavelet Transform (R-DWT) based convolutional neural network (CNN) [28]. They observed that the shift-invariance of the R-DWT approach may be utilized to quickly build high-quality CT scan classifications using their proposed strategy. A technique called as pyramid transformation may be used to accomplish the categorization of numerous images of a CT scan [29]. This method was soon adopted and became extensively used in a number of applications, including computer vision, image compression, and CT scan segmentation [30]. The pyramid transform is becoming increasingly popular for combining multiple-view clinical CT images.

The authors of [31] described the union ResNet51 technique for multiclass lung cancer classification, which enabled them to extract a significant number of critical properties [32] from segmented CT images. The authors of suggested Region Mosaicking on Laplacian Pyramids for feature extraction using Google Net as a technique for fusing CT images taken by a microscope in [33], however it was proved to be noisy. The Laplacian pyramid approach with joint averaging was then devised, which resulted in a significant improvement in the output by showing the image's rich background details.

The authors of [34] reported their results on a groundbreaking multi-modal medical CT scan categorization approach. On contrast CT images, a serial canonical correlation-based categorization of various textural, point, and geometric characteristics is performed. The authors of [35] combined basic mean filter-based preprocessing with U-Net-based segmentation. Furthermore, machine learning-based SVM is employed to differentiate between the benign and malignant lung classifications. However, this strategy requires more time for training.

According to the study, traditional approaches failed to correctly segregate the cancer-affected area, resulting in lower categorization. Machine learning methods are unable to distinguish between benign and malignant illness characteristics.

3. PROPOSED METHOD

This section provides a full study of the proposed OLDC-Net, which conducts four primary operations: HRBF-based preprocessing, UKMC segmentation, ML-DWT-based feature extraction, MSOA-based feature selection, and RCNN classification. Figure 1 depicts the proposed OLDC-Net structure, and Table 1 depicts the proposed OLDC-Net method.

3.1 HRBF Preprocessing

A high contrast image and mail-in trilateral filter has been presented as a nonlinearly single-pass filter to retain the edge of smoothing and visible detail for N-dimensional signaling in computer graphics, image processing, and computer vision applications. The trilateral filter is used to incorporate the local image statistics into the HRBF in order to locate noisy pixels in random images impacted by impulse noise.
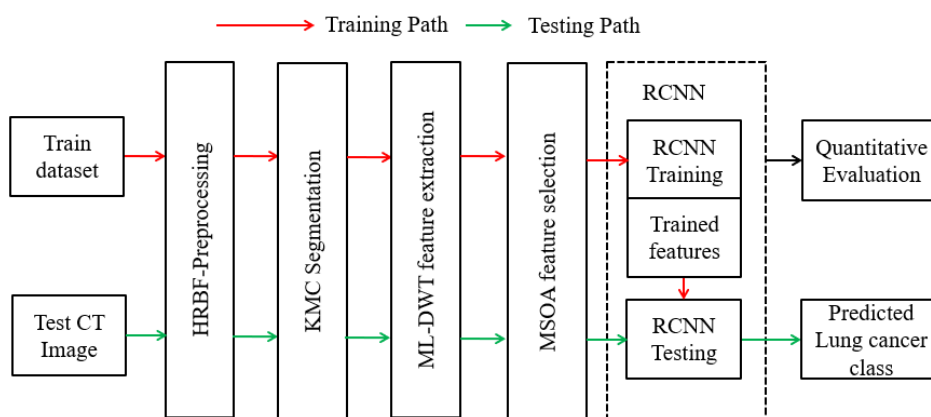
Figure 1. Proposed OLDC-Net model.

Table 1. Proposed OLDC-Net model.

Input: LIDC-IDRI dataset, test CT image **Output:** Segmented image, classified lung cancer class. **Performance measures:** Preprocessing, segmentation, classification metrics.
Step 1: Take the LIDC-IDRI training dataset and apply it to HRBF preprocessing for noise reduction and CT image improvement.
Step 2: Use UKMC segmentation to pinpoint the affected area of lung cancer.
Step 3: Run ML-DWT on the UKMC segmented results to extract precise disease-specific characteristics.
Step 4: Select optimum features using an MSOA-based bio-optimization technique.
Step 5: Run RCNN-based training, extract learned features, and assess segmentation and classification results.
Step 6: Take a look at the test CT image and repeat steps 1–5 to extract the test features.
Step 7: Run the RCNN model for testing, which predicts lung cancer classes.
Step 8: Compare the preprocessing, segmentation, and classification metrics to state-of- **Step 9:** the-art techniques.

The comprehensive preprocessing technique of CT images using HRBF is shown in Figure 2. Initially, noisy asthma CT images are sent into the quick box filter, which divides the CT

images into spectral and angular coefficients. In this case, spectral coefficients include amplitude, phase, and pitch intensities, while angular coefficients provide phase aware information. These characteristics are created by translating time to frequency conversions. The "A posteriori SNR estimate" is then applied to the original noise removed signal and noise levels. The procedure is repeated until the signal levels are enhanced in comparison to the noise levels, which may be determined using the signal to noise ratio (SNR). Finally, an increase in SNR values shows that the noise level is decreasing. The posteriori result is applied to the priori data, and the noise in the phase and pitch intensities is found using multi spectral analysis.

In this case, "A priori SNR estimate" is employed to calculate the spectrum gain while simultaneously reducing the jitters in the different gain data. The lower and higher frequency levels are identified and adjusted to increase spectral gain. The procedure is repeated many times, resulting in an enhanced gain factor. The original amplitude of the CT image is then multiplied by the gain levels, and this multiplication is employed to enhance the spectral characteristics. Finally, the obtained amplitude levels are fed into the recursive filter with the original phase angles, which produces the clean CT image.
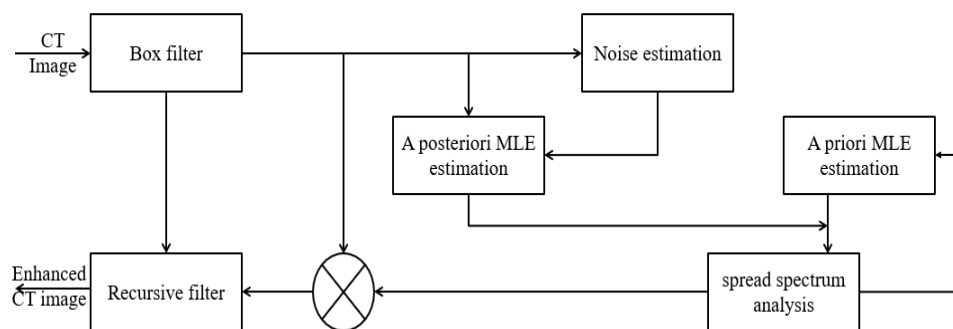

Figure 2. HRBF preprocessing

3.2 UKMC segmentation

When lung parenchyma segmentation is conducted, it is highly advantageous in finding and analyzing surrounding lesions, but it is only successful if certain methodologies and frameworks are employed. Lung parenchyma segmentation is an important pre-processing step in the CAD system's design of lung nodules from CT image sequences. An efficient thresholding method was used while constructing the OLDC-Net to minimize the complexity of lung segmentation in order to save processing time while enhancing accuracy. With the use of experimentation and data analysis, the approach was evaluated on a number of CT scans collected from the LIDC-IDRI.

In this case, the UKMC technique is used to identify brain cancer during transformation in order to partition the lung cancer area using thresholding. The initial phase in the UKMC approach is segmentation, and at the cluster centers, cost junction must be reduced, which

varies based on the memberships of user inputs. Image segmentation is the process of separating a brain cancer into several clusters depending on the area of interest exhibited in order to diagnose lung cancer. Radiologists use areas of interest, which are segments of lung images, to find anomalies such micro classifications (malignant and benign). K indicates that clustering is used to some degree in the recommended segmentation procedure. The active counter clustering approach is chosen because of its speed of operation while maintaining the highest accuracy. The UKMC strategy, as shown in Figure 3, combines the advantages of jointly possible and K means clustering techniques. The membership functions are built using a probability-based technique to enhance detection. Among those detected malignancies, the most precise cancer spots are considered as ROI. It is difficult to calculate ROI automatically. As a consequence, ROIs are generated utilizing potential cropping, which is dependent on the position of the abnormality in the original test brain tumors. The membership functions are built using a probability-based technique to enhance detection. Among the found Tumor regions, the most accurate Tumor region is considered ROI.
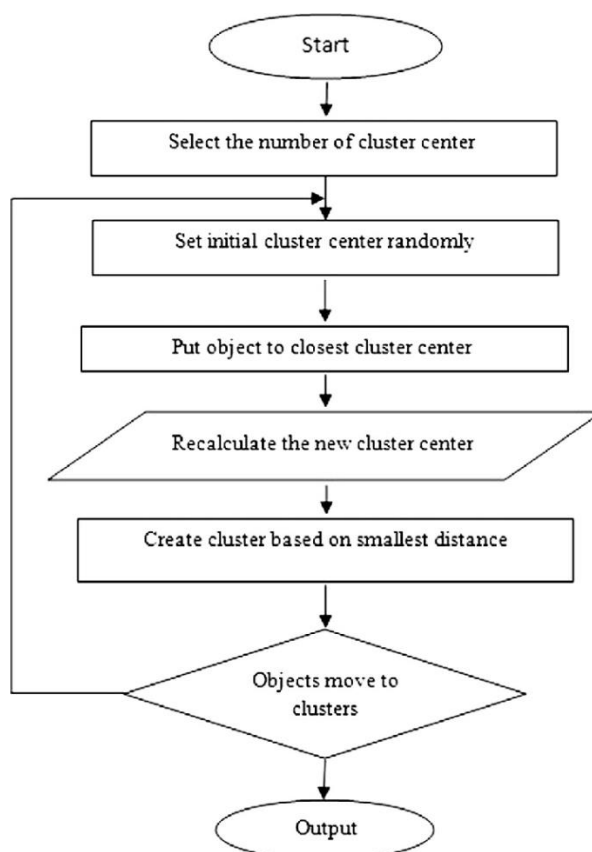

Figure 3: UKMC segmentation

3.3. Feature extraction

The wavelet indicates the decomposed frequency band of image, which refers the grouping of frequency dependent pixels of varying sizes. Further, this decomposition operation is carried

out by using complex or real-valued data with square-integrable properties. The ML-DWT is the advanced wavelet transform, which extracts more accurate features in frequency domain compared to FFT and DFT. The conventional transforms are suffering with data reduction or compression problems due to improper samplings, which are overcome in ML-DWT by introducing the edge aware frequency dependent filters. Ideally, the calculation of the ML-DWT of a signal x is accomplished by passing it through filters sequence. The deconstruction and reconstruction processes of DWT are shown in Figure 4. As a first stage, the input samples are routed via the LF channel and into the impulse response channel (g), which results in a convolution of two signals:

$$y[n] = (x * g)[n] = \sum_{k=-\infty}^{\infty} x[k]g[n - k] \qquad (1)$$

The output coefficients acquired from the LF are referred to as approximations. At the same time, the same signal is decomposed by employing the HF, which is indicated as h, and the resulting detail coefficients are referred to as details. It is critical that both the LF and HF frequencies be connected together, which is referred as quadrature mirror filter.
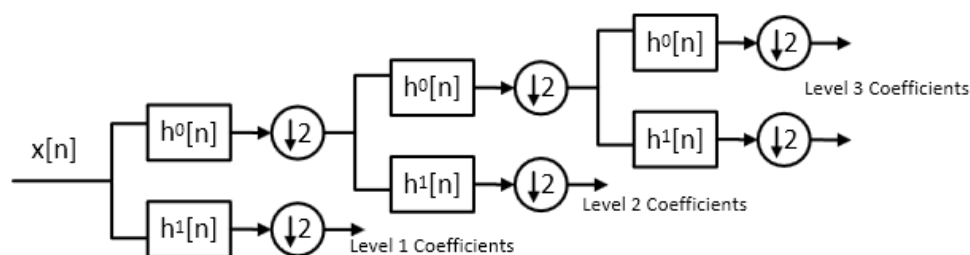

Figure 4. ML-DWT feature extraction.

Further, ML-DWT maintains the energy of the image pixels, which helped to hold the brightness and luminance properties. The color properties of original image remains unchanged by using ML-DWT. Thus, the feature extraction schemes can be effectively implemented by adopting ML-DWT for LL band-based feature extraction.

3.4 Feature selection

Moths and butterflies account for 53 percent of all species worldwide. They never want to be seen by predators during the day. They usually try to exploit food sources at night by employing the celestial triangulation method. For such an orientation, the across direction of motion is always a concern. The light source is represented by MSOA in Figure 5, and the fitness value of the objective function is taken into account as the luminous intensity of the light source. These assumptions underpin the proposed algorithm. The following strategy is based on the following features of three distinct moth species: - Pathfinders: Some moths (t) will constantly attempt to locate a new site in the optimization area using the first in, last out rule. They are continually looking for the best source of light to assist them identify the optimum route for the main swarm. Prospectors: Pathfinders always help a group of moths identify nearby light sources by following an arbitrary spiral route. Onlookers: This swarm is attempting to advance towards the best global answer (moonlight).

3.4.1 Mathematical derivation of the suggested algorithm

To adjust the control parameters of an objective function, MSOA suggests four primary steps, which are as follows: In the first stage, known as the start phase, an s-number of n-dimensional search agents are randomly assigned positions as follows:

$$x_{pq} = rand[0,1].\left(x_q^{max} - x_q^{min}\right) + x_q^{min} \qquad (2)$$

$$\forall p \in \{1,2,3, \dots \dots s\}, q \in \{1,2,3 \dots \dots n\} \qquad (3)$$

The lower and upper boundaries of the "x pq" control parameter in this example are "x_q^{max}" and "x_q^{min}," respectively. At first, the best moth from the swarm is selected based on its fitness value. Furthermore, the best group of moths, selected as the light's mainstream and acting as pathfinders, are ahead of prospectors and watchers. At first, the best moth from the swarm is selected based on its fitness value. Furthermore, the finest moths, selected as the majority of light and functioning as pathfinders, outnumber prospectors and onlookers. The pathfinders' positions are updated in the following step, termed reconnaissance, which lasts five stages. In the diversity index-based crossover strategy, a distinct concept is used to identify the crossover location. A normalized dispersion degree parameter is used in this crossover approach. For the first I number of iterations, the standardized dispersion degree of the "ζ_q^i" people in the "$x_q^{\vec{i}}$ " dimension is as follows:

$$\zeta_q^i = \frac{\sqrt{\frac{1}{r_t}\sum_{p=1}^{\eta_t}\left(x_{pq}^i - x_q^{\vec{i}}\right)^2}}{x_q^{\vec{i}}} \qquad (4)$$

Where $x_q^{\vec{i}} = \frac{1}{\gamma_t} \sum_{p=1}^{\eta_t} x_{p=1}^i$ and 'γ_t' is the number of pathfinders and may be written as a variation coefficient helpful for determining relative dispersion.

$$\gamma^t = \frac{1}{n}\sum_{q=1}^{d} \zeta_q^i \qquad (5)$$

Pathfinder grieves from low degree of dispersion moth to traverse via sites 'bp 'as follows for a certain region:

$$q\epsilon b_p \, if \, \rho_q^i \le \xi^1 \qquad (6)$$

The recommended technique animatedly modified the set of transverse points. The second phase employs levy flight based on a stable distribution. Step 2 also employs the heavy-tailed probability density function (PDF) and anomalous diffusion. Sub trail-vectors [v i1,v i2,v i3,........v in] are created in the third phase utilizing host vectors [x i1,x i2,x i3,........x in] and donor vectors. To get a full trail solution, the host vector changes its location using a crossover operation on the pathfinder solution, which occurs in the 'fourth step' and is represented by:

$$U_{qi}^t = \begin{cases} v_{qi}^t \, if \, i\epsilon c_i \\ u_{qi}^t \, if \, i \notin c_i \end{cases} \qquad (7)$$

Finally, in the fifth stage, known as the 'transverse orientation phase,' the number of prospectors reduces as follows:

$$\eta_f = round((\eta - \eta_p) \times (1 - r)) \qquad (8)$$

Here (r = t /T);'t' is the current iteration and 'T' is the number of iterations; and "η_f" is the total number of prospectors and pathfinders. The lowest luminous sources are found in the onlooker. As a result, in the last stage (Celestial navigation), the moths in this group attempt to travel towards the shiniest solution. Onlooker moths use Gaussian walks and associative learning techniques to update their location. The new location of the onlooker moth is updated via the Gaussian walks technique as follows:

$$u_j^{t+1} = u_j^t + \sigma 1 + \left[\sigma 2 \times fit_h^t - \sigma 3 \times u_j^t\right]; \forall j \in \{1,2,3, \dots \gamma G\} \qquad (9)$$

The changed location of the onlooker moth is obtained by using the associative learning mechanism:

$$q_j^{t+1} = q_j^t + 0.001. H\left[q_j^t - q_j^{min}.u_j^{max} - u_j^t\right] + \left(1 - \frac{h}{H}\right).s_1.\left(f \ it \ t_q^t - u_j^t\right) + \\ \frac{2h}{H}.s_2(f \ it \ t_h^t - q_j^t \qquad (10)$$

Here 2h/H is considered a social factor and (1-h/H) is considered a cognitive element; s1, s2 are the two variables that fluctuate within the range of (0, 1).

Despite the fact that MSOA is a recently designed nature-inspired met heuristics method, it has several limitations such as sluggish convergence and local optimality. To accelerate the convergence rate, chaos is injected into MSA to increase its variety. Six distinct feature selection maps were used in this study to determine the ideal location of prospectors for increasing exploration and exploitation capacity.
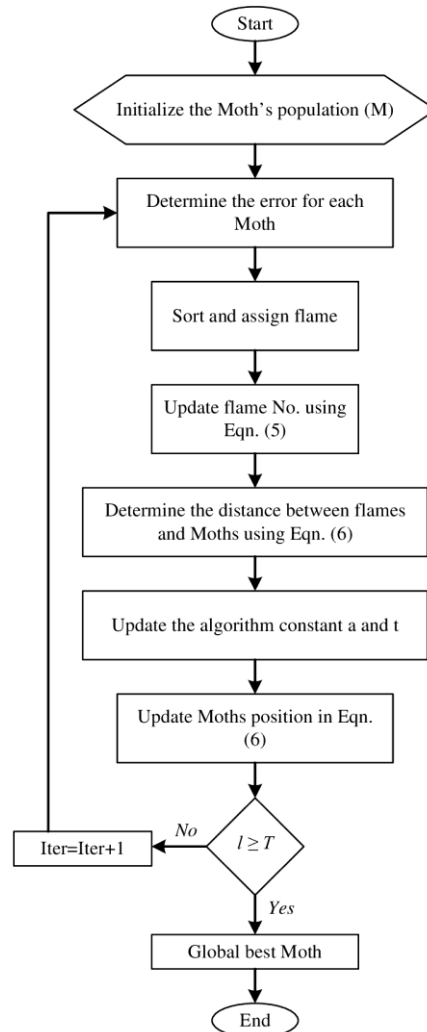
Figure 5. Flowchart of MSOA.

3.4.3 MSOA feature selection maps

The feature selection behavior of many nonlinear systems has recently been a prominent topic in several areas such as chaos management, pattern recognition, and artificial intelligence optimization theory. The primary objective for including a feature selection map into the MSOA algorithm is to achieve excellent equality between exploitation and exploration throughout iteration. In MSA, feature selection mapping gives I quasi stochasticity, (ii) sensitivity to the starting condition, and (iii) periodicity. The number of prospectors "η_f" 'represented in (11) is heavily influenced by in the transverse orientation stage of the moth swarm method, which decreases linearly with the number of iterations. However, in order to achieve a fair balance between exploitation and exploration throughout iteration, the value of 'r' in the proposed CMSA technique affects feature selection, allowing for exploration in the last phases. After evaluating the performance of several feature selection maps, the authors

discovered that include the 'singer' feature selection map increases the convergence rate faster than all other feature selection functions, and so equation (11) may be rewritten as:

$$\eta_f = round\left((\eta - \eta_p) \times (1 - r)\right) wherever = \frac{t}{T} + c_i^{norm} \qquad (11)$$

3.5 Classification

The following are the stages involved in training an RCNN:

- The network is given a single time step of the input. The current state is then calculated by combining the current input with the prior state. For the following time step, this present state becomes ht-1, and so on.

- Once all of the time steps have been completed, the output is calculated using the final current state.

- The created output is then compared to the actual output (the target output), and an error is generated.

- The mistake is subsequently back-propagated to the network, which updates the weights and therefore trains the network (RCNN). As a result, the mistake amount is distributed across the connections.

The RCNN models are widely used in many medical image processing applications including multi class lung cancer classification. It is a kind of efficient identification approach that has lately gotten a lot of attention because of its effectiveness. The advantage of RCNNs is that they are simpler to train and have a much smaller number of parameters than fully linked networks.

Figure 6 presents the detailed layer wise architecture of proposed RCNN model and Table 6 presents the properties of each layer of RCNN model. Here, convolution layer is used to extract the deep features using weighted kernel. There are two primary sources of error in feature extraction: the neighborhood size constraint produced and the estimated error in the convolution layer parameter estimation generated by the mean deviation. When using mean pooling, the first mistake may be reduced while still keeping more CT scan background information. With maximum pooling, it is possible to lower the second error while maintaining more texture information.
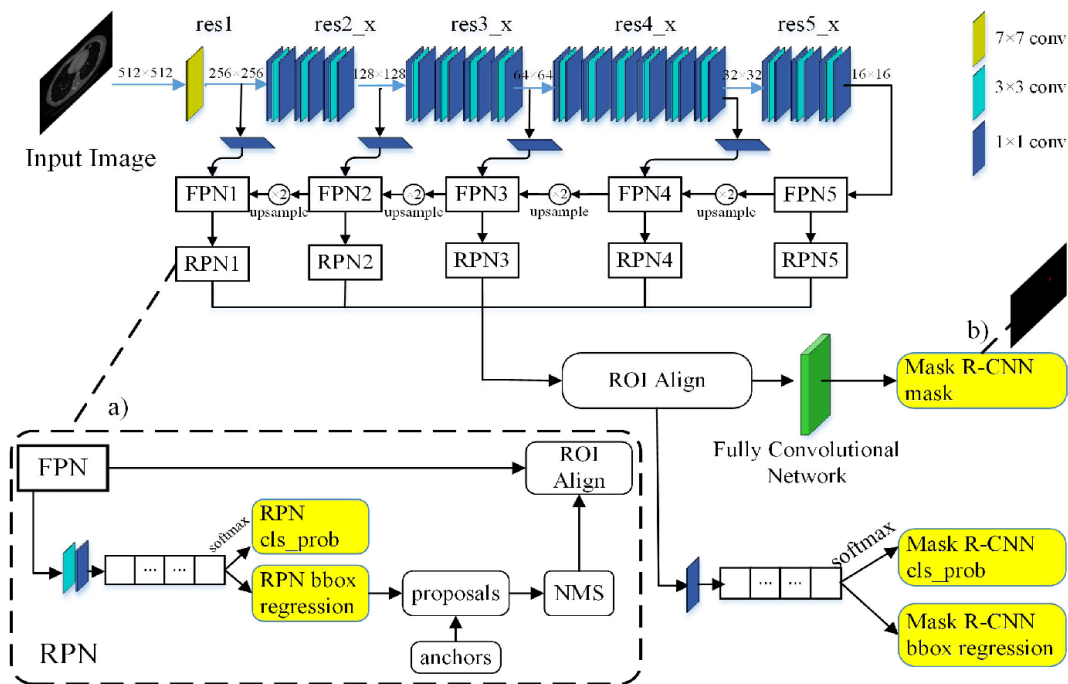
Figure 6. RCNN classification

Then, max pooling layer is used to reduce the number features by selecting the best value in each kernel. The convolution and max-pooling layers are repeated multiple times to generate the best features with low computational complexity. Further, fully connected layer is used to map the input to output features by maintaining all the neuron interconnections. Finally. SoftMax classifier is used to classify the benign and malignant classes from test features.

4. RESULTS AND DISCUSSIONS

This section provides a thorough examination of simulation findings, including comparisons to state-of-the-art methodologies. For implementation, both the suggested OLDC-Net and traditional approaches used the same dataset. Furthermore, an ablation study of the proposed OLDC-Net was carried out to assess the superiority of each approach.

4.1 Datasets

The Lung Image Database Consortium's (LIDC-IDRI) image collection includes diagnostic and screening thoracic CT images with marked-up annotated lesions. It is a web-based global resource for the development, training, and evaluation of CAD techniques for lung cancer detection and diagnosis. This public-private partnership, initiated by the National Cancer Institute (NCI), advanced by the Foundation for the National Institutes of Health (FNIH), and supported by the Food and Drug Administration (FDA) through active participation, demonstrates the success of a consortium built on consensus. This data set, which contains 1018 cases, was generated in partnership with seven academic institutions and eight medical imaging companies. Each subject includes images from a clinical thoracic CT scan as well as

an XML file with the results of a two-phase image annotation method performed by four qualified thoracic radiologists. Each radiologist individually reviewed each CT image during the first blinded-read phase and labelled lesions as "nodule > or =3 mm," "nodule 3 mm," or "non-nodule > or =3 mm." Each radiologist independently reviewed their own markings, as well as the anonymized marks of the three other radiologists, during the subsequent unblinded-read phase to establish a final verdict. The goal of this technique was to find as many lung nodules as possible on each CT image without resorting to forced consensus.

4.2 Subjective analysis

This section depicts the visual subjective analysis based on preprocessing and segmentation. Figure 7 depicts the HRBF preprocessing output images, which successfully removed various forms of background noises and improved the cancer-presented region. HRBF additionally enhances the spatial and texture qualities of pixels.
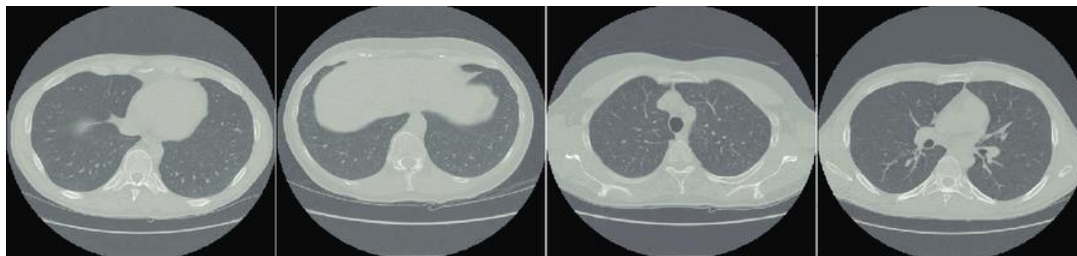
(a) Input CT images
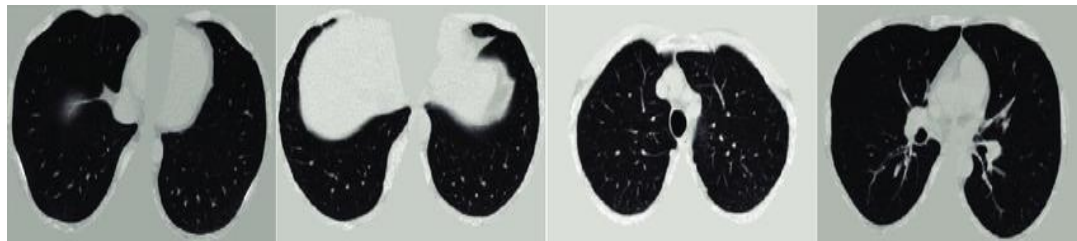
(b) HRBF preprocessed images

Figure 7. Preprocessing using HRBF

Figure 8 depicts the segmented output images produced by the UKMC technique. Furthermore, the first and third columns are the input images, while the second and fourth columns are the segmented images. The UKMC approach described here correctly segments the tumor zone. Figure 9 compares the visual performance of lung CT image segmentation with standard techniques. When compared to standard image processing techniques such as UKMC, FCM, and MOTSU, the suggested UKMC segmentation approach resulted in improved localization of the cancer-affected area. Traditional approaches led in inferior localization of cancer regions, resulting in worse classification performance.
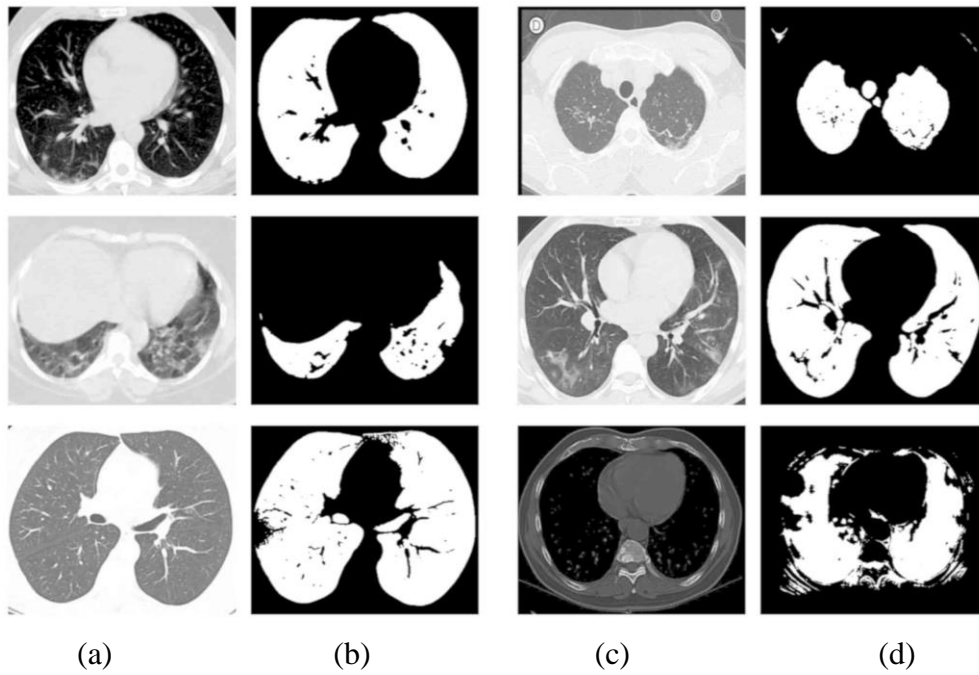
| | | | |
| (a) | (b) | (c) | (d) |

Figure 8. UKMC based segmented output images.

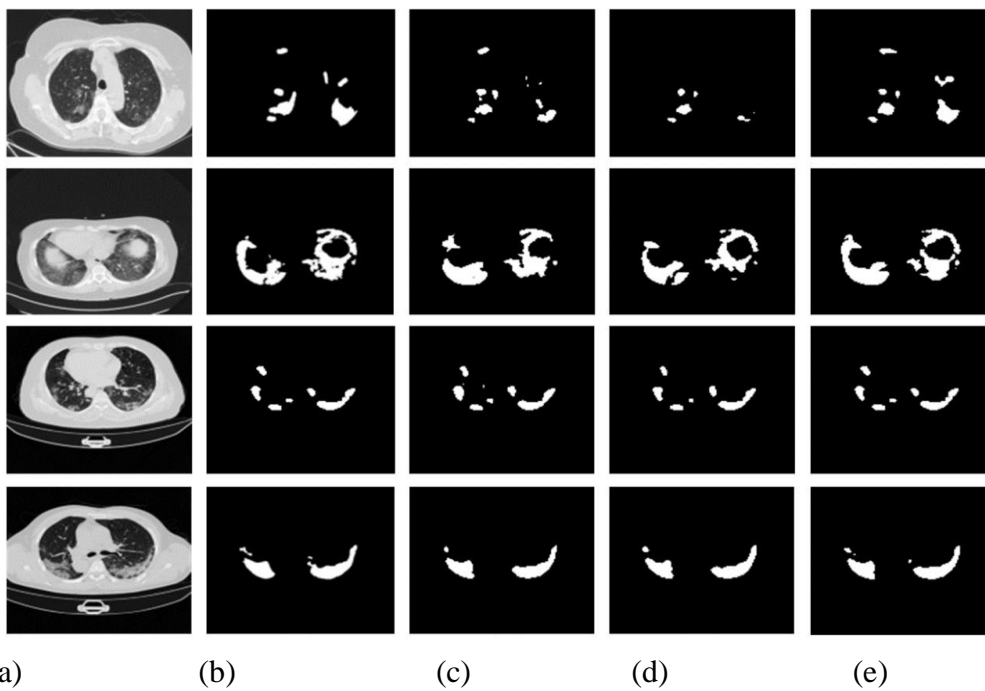| | | | | |
| (a) | (b) | (c) | (d) | (e) |

Figure 9. CT image segmented images using various approaches, (a) input, (b) UKMC [26] (c) FCM [23], (d) MOTSU [24], and (e) proposed HMF.

4.3 Objective performance

This section gives the detailed analysis of subjective analysis of proposed OLDC-Net with conventional models using various metrics such as peak signal to noise ratio (PSNR), structural similarity index metric (SSIM), mean square error (MSE), entropy, standard deviation (STD), and mutual information (MI).

Table 2. Preprocessing methods performance comparison

Method	PSNR	SSIM	MSE	Entropy	STD	MI
Mean filter [11]	48.42	0.236	0.0748	5.33	0.966	3.91
Median filter [13]	51.80	0.259	0.0646	5.70	0.955	4.40
Gaussian filter [14]	52.93	0.358	0.0374	5.74	0.720	4.64
Bilateral filter [15]	53.67	0.412	0.0137	6.70	0.539	6.75
Trilateral filter [16]	54.41	0.604	0.0098	7.26	0.473	6.90
NLM [17]	54.45	0.873	0.0076	8.11	0.351	7.47
Proposed HRBF	57.64	0.913	0.0012	11.23	0.054	10.27

Table 2 compares the proposed HRBF strategy to traditional approaches such as the Mean filter [11], Median filter [13], Gaussian filter [14], Bilateral filter [15], Trilateral filter [16], and NLM [17]. Furthermore, when compared against all current approaches, the suggested HRBF outperformed them all. Figure 10 depicts a graphical depiction of the performance comparison of preprocessing techniques.
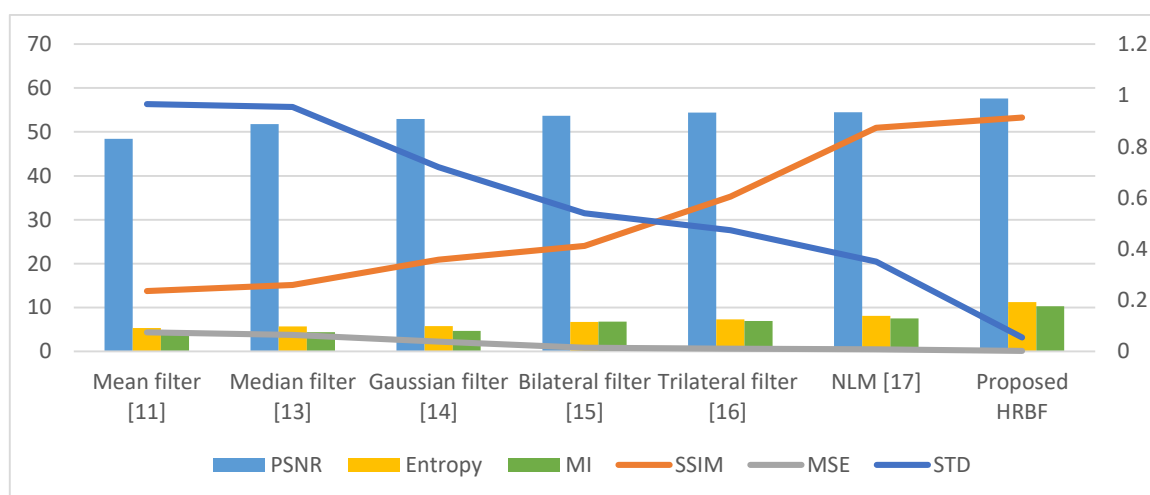

Figure 10. Graphical representation of preprocessing methods performance comparison.

Table 3 compares the proposed UKMC segmentation method's performance to those of existing approaches like Morphological [20], Adaptive Thresholding [21], FCM [23], and MOTSU [24]. Furthermore, the proposed UKMC exceeds all performance measures such as segmentation accuracy (SACC), segmentation sensitivity (SSEN), segmentation specificity

(SSPE), segmentation F1-measure (SF1M), segmentation recall (SRE), and segmentation precision (SRE) (SPR). Figure 11 shows a graphical representation of the performance of segmentation methods.

Table 3. Segmentation methods performance comparison.

Method	SACC	SSEN	SSPE	SF1M	SRE	SPR
Morphological [20]	92.41	90.31	90.13	90.10	92.49	90.21
Adaptive Thresholding [21]	92.62	93.22	91.66	92.19	93.13	90.27
FCM [23]	93.25	93.64	92.72	93.18	93.66	94.48
MOTSU [24]	94.44	94.81	94.16	93.36	93.83	96.89
Proposed UKMC	98.35	98.86	98.90	98.38	98.91	98.96

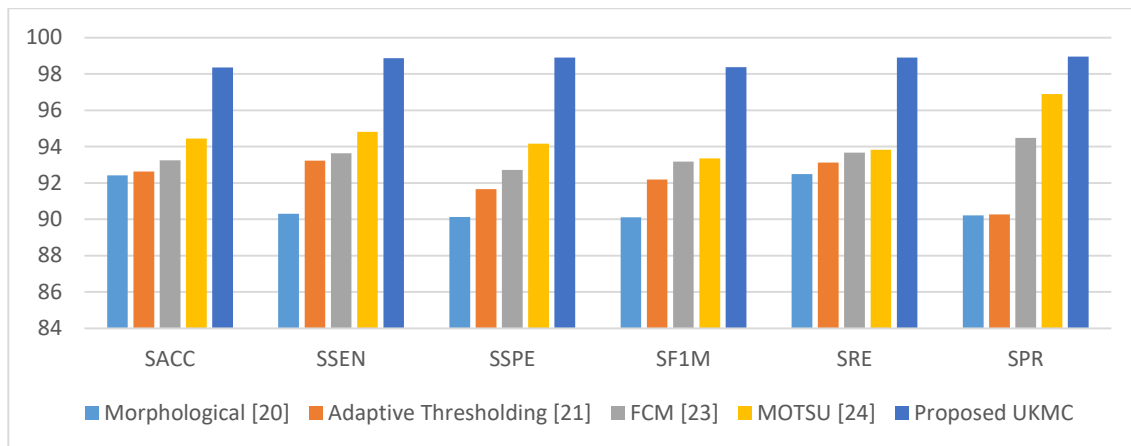**Figure 11. Graphical representation of segmentation methods performance comparison.**

Table 4. Classification methods performance comparison.

Method	CACC	CSEN	CSPE	CF1M	CRE	CPR	CAUC
SVM [27]	88.30	89.21	88.02	88.06	89.78	88.35	88.49
CNN [28]	88.33	91.53	92.90	90.91	89.87	89.54	88.83
AlexaNet [30]	90.35	92.44	93.41	91.32	91.13	89.70	91.84
ResNet51 [31]	93.83	93.08	94.58	91.59	92.93	92.12	93.28
GoogleNet [33]	94.79	95.68	94.80	92.97	94.84	95.12	93.30
U-Net with SVM [35]	96.00	95.81	94.88	93.83	96.00	96.03	96.18
Proposed OLDC-Net	98.31	98.12	97.48	98.38	98.27	98.29	98.98

Table 4 contrasts the proposed OLDC-Net performance with traditional techniques such as SVM [27], CNN [28], AlexaNet [30], ResNet51 [31], GoogleNet [33], and U-Net with SVM [35]. Furthermore, the proposed OLDC-Net outperforms other networks in terms of classification accuracy (CACC), classification sensitivity (CSEN), classification specificity

(CSPE), classification F1-measure (CF1M), classification recall (CRE), classification precision (CPR), and classification area under curve (CAUC). Figure 12 depicts a graphical depiction of the performance comparison of categorization algorithms.
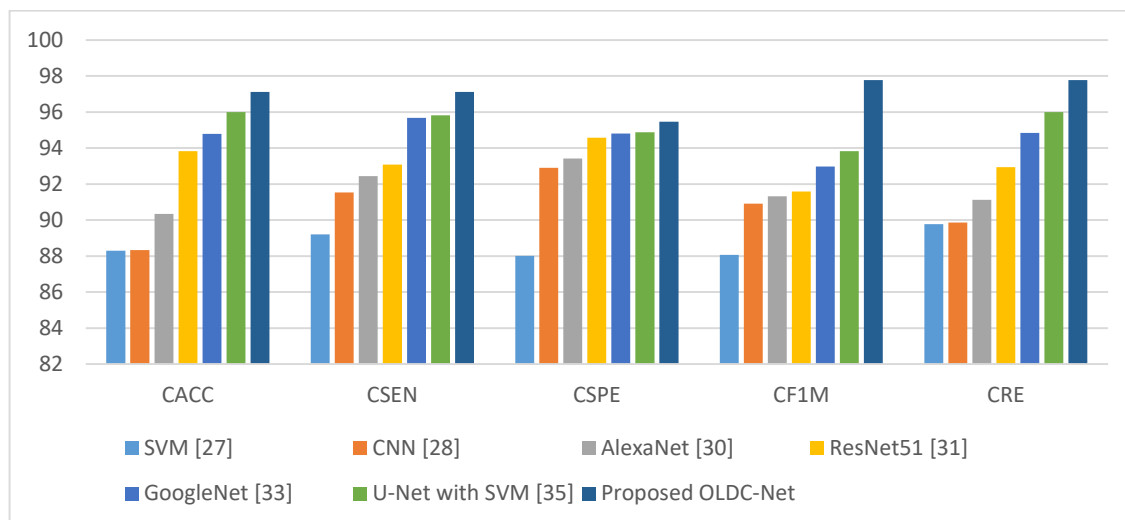

Figure 12. Graphical representation of classification methods performance comparison.

5. CONCLUSION

This study proposes a deep learning and bio-optimization-based OLDC-Net model for lung cancer segmentation and multiclass classification. Initially, HRBF was utilized to minimize various forms of noise from CT source images while simultaneously improving the disease-affected area. The disease-affected area was then localized using UKMC segmentation. Those, ML-DWT was also utilized to extract deep seismic features from segmented images. Furthermore, an MSOA-based bio-optimization strategy was employed to choose deep interdependence characteristics with disease-specific probability dependent features. Finally, utilizing optimum features, the RCNN model was applied to categories CT lung images into benign and malignant groups. The simulation results reveal that the suggested OLDC-Net outperformed standard techniques in terms of preprocessing, segmentation, and classification. This research may be expanded with more optimization approaches and transfer learning models for segmentation and classification.

References

1) Sharif, Muhammad Irfan, et al. "A comprehensive review on multi-organs tumor detection based on machine learning." Pattern Recognition Letters 131 (2020): 30-37.

2) Shakeel, P. Mohamed, M. A. Burhanuddin, and Mohammad Ishak Desa. "Automatic lung cancer detection from CT image using improved deep neural network and ensemble classifier." Neural Computing and Applications (2020): 1-14.

3) Asuntha, A., and Andy Srinivasan. "Deep learning for lung Cancer detection and classification." Multimedia Tools and Applications 79.11 (2020): 7731-7762.

4) Yu, Kun-Hsing, et al. "Reproducible machine learning methods for lung cancer detection using computed tomography images: Algorithm development and validation." Journal of medical Internet research 22.8 (2020): e16709.

5) Bhatia, Siddharth, Yash Sinha, and Lavika Goel. "Lung cancer detection: a deep learning approach." Soft Computing for Problem Solving. Springer, Singapore, 2019. 699-705.

6) Schwyzer, Moritz, et al. "Automated detection of lung cancer at ultralow dose PET/CT by deep neural networks–initial results." Lung Cancer 126 (2018): 170-173.

7) Lakshmanaprabu, S. K., et al. "Optimal deep learning model for classification of lung cancer on CT images." Future Generation Computer Systems 92 (2019): 374-382.

8) Ardila, Diego, et al. "End-to-end lung cancer screening with three-dimensional deep learning on low-dose chest computed tomography." Nature medicine 25.6 (2019): 954-961.

9) Riquelme, Diego, and Moulay A. Akhloufi. "Deep learning for lung cancer nodules detection and classification in CT scans." AI 1.1 (2020): 28-67.

10) Chaunzwa, T. L., Hosny, A., Xu, Y., Shafer, A., Diao, N., Lanuti, M., ... & Aerts, H. J. (2021). Deep learning classification of lung cancer histology using CT images. Scientific reports, 11(1), 1-12.

11) Lee, J. H., Sun, H. Y., Park, S., Kim, H., Hwang, E. J., Goo, J. M., & Park, C. M. (2020). Performance of a deep learning algorithm compared with radiologic interpretation for lung cancer detection on chest radiographs in a health screening population. Radiology, 297(3), 687-696.

12) Toğaçar, Mesut, Burhan Ergen, and Zafer Cömert. "Detection of lung cancer on chest CT images using minimum redundancy maximum relevance feature selection method with convolutional neural networks." Biocybernetics and Biomedical Engineering 40.1 (2020): 23-39.

13) Bhandary, Abhir, et al. "Deep-learning framework to detect lung abnormality–A study with chest X-Ray and lung CT scan images." Pattern Recognition Letters 129 (2020): 271-278.

14) Avanzo, M., Stancanello, J., Pirrone, G., & Sartor, G. (2020). Radiomics and deep learning in lung cancer. Strahlentherapie und Onkologie, 196(10), 879-887.

15) Huang, P., Lin, C. T., Li, Y., Tammemagi, M. C., Brock, M. V., Atkar-Khattra, S., ... & Lam, S. (2019). Prediction of lung cancer risk at follow-up screening with low-dose CT: a training and validation study of a deep learning method. The Lancet Digital Health, 1(7), e353-e362.

16) Singh, Gur Amrit Pal, and P. K. Gupta. "Performance analysis of various machine learning-based approaches for detection and classification of lung cancer in humans." Neural Computing and Applications 31.10 (2019): 6863-6877.

17) Nasrullah, N., Sang, J., Alam, M. S., Mateen, M., Cai, B., & Hu, H. (2019). Automated lung nodule detection and classification using deep learning combined with multiple strategies. Sensors, 19(17), 3722.

18) Jakimovski, G., & Davcev, D. (2019). Using double convolution neural network for lung cancer stage detection. Applied Sciences, 9(3), 427.

19) Masood, Anum, et al. "Computer-assisted decision support system in pulmonary cancer detection and stage classification on CT images." Journal of biomedical informatics 79 (2018): 117-128.

20) Wang, Shuo, et al. "Predicting EGFR mutation status in lung adenocarcinoma on computed tomography image using deep learning." European Respiratory Journal 53.3 (2019).

21) Kadir, T., & Gleeson, F. (2018). Lung cancer prediction using machine learning and advanced imaging techniques. Translational lung cancer research, 7(3), 304.

22) Ruan, Jingru, et al. "Development of deep learning-based automatic scan range setting model for lung cancer screening low-dose CT imaging." Academic Radiology (2022).

23) Punithavathy, K., Sumathi Poobal, and M. M. Ramya. "Performance evaluation of machine learning techniques in lung cancer classification from PET/CT images." FME Transactions 47.3 (2019): 418-423.

24) Polat, Huseyin, and Homay Danaei Mehr. "Classification of pulmonary CT images by using hybrid 3D-deep convolutional neural network architecture." Applied Sciences 9.5 (2019): 940.

25) Thakur, Shailesh Kumar, Dhirendra Pratap Singh, and Jaytrilok Choudhary. "Lung cancer identification: a review on detection and classification." Cancer and Metastasis Reviews 39.3 (2020): 989-998.

26) Park, S., Lee, S. M., Do, K. H., Lee, J. G., Bae, W., Park, H., ... & Seo, J. B. (2019). Deep learning algorithm for reducing CT slice thickness: effect on reproducibility of radiomic features in lung cancer. Korean journal of radiology, 20(10), 1431-1440.

27) Ozdemir, Onur, Rebecca L. Russell, and Andrew A. Berlin. "A 3D probabilistic deep learning system for detection and diagnosis of lung cancer using low-dose CT scans." IEEE transactions on medical imaging 39, no. 5 (2019): 1419-1429.

28) Masood, A., Yang, P., Sheng, B., Li, H., Li, P., Qin, J., ... & Feng, D. D. (2019). Cloud-based automated clinical decision support system for detection and diagnosis of lung cancer in chest CT. IEEE journal of translational engineering in health and medicine, 8, 1-13.

29) Qin, R., Wang, Z., Jiang, L., Qiao, K., Hai, J., Chen, J., ... & Yan, B. (2020). Fine-grained lung cancer classification from PET and CT images based on multidimensional attention mechanism. Complexity, 2020.

30) Chao, H., Shan, H., Homayounieh, F., Singh, R., Khera, R. D., Guo, H., ... & Yan, P. (2021). Deep learning predicts cardiovascular disease risks from lung cancer screening low dose computed tomography. Nature communications, 12(1), 1-10.

31) Gerard, S. E., Patton, T. J., Christensen, G. E., Bayouth, J. E., & Reinhardt, J. M. (2018). FissureNet: a deep learning approach for pulmonary fissure detection in CT images. IEEE transactions on medical imaging, 38(1), 156-166.

32) Zhou, T., Lu, H., Yang, Z., Qiu, S., Huo, B., & Dong, Y. (2021). The ensemble deep learning model for novel COVID-19 on CT images. Applied Soft Computing, 98, 106885.

33) Khan, M. A., Rubab, S., Kashif, A., Sharif, M. I., Muhammad, N., Shah, J. H., ... & Satapathy, S. C. (2020). Lungs cancer classification from CT images: An integrated design of contrast based classical features fusion and selection. Pattern Recognition Letters, 129, 77-85.

34) Wang, W., Liu, F., Zhi, X., Zhang, T., & Huang, C. (2020). An integrated deep learning algorithm for detecting lung nodules with low-dose CT and its application in 6G-enabled internet of medical things. IEEE Internet of Things Journal, 8(7), 5274-5284.

35) Suresh, S., & Mohan, S. (2020). ROI-based feature learning for efficient true positive prediction using convolutional neural network for lung cancer diagnosis. Neural Computing and Applications, 32(20), 15989-16009.